

Graphene-modified Ru nanocatalyst for low-temperature hydrogenation of carbonyl groups

Jingjing Tan, Jinglei Cui, Xiaojing Cui, Tiansheng Deng, Xianqing Li, Yulei Zhu, and Yong-Wang Li

ACS Catal., **Just Accepted Manuscript** • DOI: 10.1021/acscatal.5b02170 • Publication Date (Web): 05 Nov 2015

Downloaded from <http://pubs.acs.org> on November 9, 2015

Just Accepted

“Just Accepted” manuscripts have been peer-reviewed and accepted for publication. They are posted online prior to technical editing, formatting for publication and author proofing. The American Chemical Society provides “Just Accepted” as a free service to the research community to expedite the dissemination of scientific material as soon as possible after acceptance. “Just Accepted” manuscripts appear in full in PDF format accompanied by an HTML abstract. “Just Accepted” manuscripts have been fully peer reviewed, but should not be considered the official version of record. They are accessible to all readers and citable by the Digital Object Identifier (DOI®). “Just Accepted” is an optional service offered to authors. Therefore, the “Just Accepted” Web site may not include all articles that will be published in the journal. After a manuscript is technically edited and formatted, it will be removed from the “Just Accepted” Web site and published as an ASAP article. Note that technical editing may introduce minor changes to the manuscript text and/or graphics which could affect content, and all legal disclaimers and ethical guidelines that apply to the journal pertain. ACS cannot be held responsible for errors or consequences arising from the use of information contained in these “Just Accepted” manuscripts.



Graphene-modified Ru nanocatalyst for low-temperature hydrogenation of carbonyl groups

Jingjing Tan, †,‡ Jinglei Cui, †,‡ Xiaojing Cui, † Tiansheng Deng, † Xianqing Li, § Yulei Zhu*, †, §, Yongwang Li †, §

† State Key Laboratory of Coal Conversion, Institute of Coal Chemistry, Chinese Academy of Sciences, Taiyuan 030001, P. R. China.

‡ University of Chinese Academy of Sciences, Beijing 100049, P.R. China.

§ Synfuels China Co. Ltd, Beijing, 101407, P.R. China.

ABSTRACT: Low-temperature efficient hydrogenation of C=O bonds in various compounds, which is one of the most important processes for producing fuels and chemicals, is of fundamental interest but remains a significant challenge. The primary problem is lacking of heterogeneous catalyst systems which are high active at ambient or low temperatures. This paper describes an efficient strategy for designing low-temperature hydrogenation catalyst. Ru nanoparticles supported on reduced graphene oxide (Ru/RGO) show remarkable efficiency for hydrogenation of levulinic acid into γ -valerolactone at temperatures as low as -10 °C. The catalyst is also highly active towards low-temperature hydrogenation of C=O bonds in other carbonyl compounds into C-OH bonds, such as furfural, propionaldehyde, 2-pentanone, hydroxyacetone, acetone, acetophenone, cyclohexanone and benzophenone. XPS and *in situ* FT-IR demonstrate that the electron transfer between Ru⁰ and RGO leads to the formation of electron-rich state of Ru⁰ nanoparticles that are highly effective for activating C=O bonds.

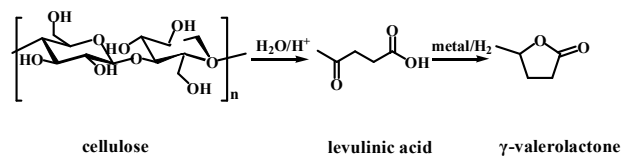
KEYWORDS: Graphene; hydrogenation; low-temperature; levulinic acid; γ -valerolactone; water

1. Introduction

The efficient hydrogenation or oxidation at ambient and lower temperatures on heterogeneous metal catalysts is highly desirable but challenging. This problem can be tackled through the development of efficient catalyst systems, especially the design of active metal sites. The primary strategies include the application of noble metals that are naturally effective at low temperatures, the reduction of metal dimension to subnano or atomic levels¹⁻⁵, the modification of chemistry of metal centers by ligands⁶⁻⁸, and the morphology control for exposing specific metal plane(s)⁹⁻¹³. In addition, it is a common and convenient method for supported metal catalysts to modify the properties of supports to produce highly active metal crystals¹⁴⁻¹⁷.

Since its discovery, graphene has attracted increasing attentions. It is a two-dimensional single-layer sheet of graphite with π -electrons fully delocalized on the graphitic plane¹⁸⁻²³. It also has the unusual ballistic electron transport, anomalous integer quantum Hall effect at room temperature and fractional quantum Hall effect at low temperatures²⁴⁻²⁷. The unique electronic properties of graphene suggest its great potential as a new carbon support for modifying the structure and chemistry of metal nanoparticles. Recent studies have demonstrated that the two-dimensional structure of graphene facilitates the hy-

bridization between graphene sp^2 -states and the d_{sp} -states of metal nanoparticles, favoring the electron feedback between graphene sheet and metal sites. Such an electron feedback is demonstrated to promote the averaged d -band center of the metal particle shifting towards its Fermi level²⁸⁻³². Based on the above understandings, we hypothesize that in the catalysis process, such a shift would ease the electron transferring between the metal sites and the reactant molecules, suggesting a superior catalytic activity.



Scheme 1 Reaction pathways from biomass to GVL

As one of the key catalytic processes in the biomass utilization, the hydrogenation of biomass-derived levulinic acid (LA) that is a versatile and renewable platform molecule primarily produced from cellulose³³⁻³⁵, into γ -valerolactone (GVL) has attracted many attentions (Scheme 1)³⁶. Many catalyst systems, including non-noble metals (Cu-, Ni- and Co) and noble metals (Pt, Pd, Ru) supported catalysts, have been reported to catalyze the hydrogenation of LA into GVL efficiently³⁷⁻⁴⁴. However,

Table 1 Hydrogenation of levulinic acid catalyzed by various catalysts^a

Entry	Cat.	T/°C	LA conv.%	GVL select.%	t/h
1	Ru/RGO	40	100	99.9	2
2	Graphite ^b	40	0	-	2
3	GO ^b	40	0	-	2
4	RGO ^b	40	1.2	99.9	2
5	Ru/Graphite	40	16.2	99.9	2
6	Ru/AC	40	55.8	99.9	2
7	Ru/TiO ₂	40	28.8	99.9	2
8	Ru/RGO	30	100	99.9	5
9	Ru/RGO	20	100	99.9	8
10	Ru/RGO	0	93.2	99.9	12
11	Ru/AC	0	3.2	99.9	12
12	Ru/RGO	-10	70.6	99.9	12
13	Ru/AC	-10	0	-	12

^a: Reduction condition: 150 °C, 4 MPa H₂, 2 h, in the presence of 14.94 g water, in the Teflon-lined steel autoclave vessel; Reaction condition: LA (2 g, 17.2 mmol), 15 g mixture of 2 wt% Ru/support catalyst and water (60 mg 2 wt% Ru/support); H₂, 4 MPa; ^b: 15 g mixture of catalyst and water (60 mg catalyst). The carbon balance for each run exceeded 96%. The LA solution did not freeze at the temperature of -10 °C for 24 h.

drastic reaction conditions are required to obtain high GVL yield over non-noble catalysts. Furthermore, the metal leaching in liquid acid media for these catalysts, especially Cu catalysts, leads to the deactivation of catalysts. In contrast, noble metal supported catalysts, particularly Ru supported catalyst, displayed higher catalytic efficiency and better stability in the aqueous hydrogenation of carbonyl groups. The optimal temperature windows for LA hydrogenation are above 70 °C^{8, 38-43}. In this paper, reduced graphene oxide (RGO) was chosen as the support to modify the hydrogenation activity of Ru catalysts. Ru/RGO exhibits superior activity and selectivity in the low-temperatures hydrogenation of LA (as low as -10 °C) and other carbonyl compounds.

2. Results and discussion

Initially, Ru/RGO catalyst, GO, RGO, graphite and Ru/graphite were tested for the hydrogenation of LA (11.8 wt%) in water at 40 °C. LA was completely converted and a nearly 100% selectivity toward GVL was obtained over Ru/RGO within 2 h. (Table 1 entry1 and Figure S1). In contrast, graphite and GO were inactive towards LA hydrogenation (entries 2-3), while a negligible conversion of LA was observed with RGO as the catalyst (entry 4). Therefore, the Ru sites account for the catalytic hydrogenation performance. A low conversion of LA was obtained when graphite as the support (entry 5). Besides, active carbon (AC) was chosen as a representative carbon support, and Ru/AC catalyst has similar distribution of surface oxygenic functional groups to that of Ru/RGO (Figure S2 and Table S1). The Ru/AC catalyst appears lower activity than Ru/RGO catalyst. The Ru/TiO₂ cata-

lyst which has been demonstrated to be effective for LA hydrogenation at 70 °C was also tested^{44a}. However, its activity is much lower at 40 °C. This result suggests the higher efficiency of Ru/RGO catalyst for low-temperature hydrogenation of LA. The catalytic performances of Ru/RGO were further investigated at lower temperatures (30 °C and 20 °C) (Table 1 and Figure S1). Ru/RGO displays high activities at ambient temperatures (30 °C and 20 °C), whereas a significant decrease in the activity was found for Ru/AC (Figure S1). The Ru/AC catalyst is unable to catalyze LA hydrogenation when the reaction temperature was lowered to -10 °C. Surprisingly, the Ru/RGO catalyst shows considerable activity at -10 °C, which are, to date, not reported in the literature concerning heterogeneous metal-catalyzed hydrogenation processes. These results show that the Ru/RGO catalyst has a superior ability to catalyze the hydrogenation of LA at low temperatures.

The turnover frequencies (TOF) and the apparent activation energies (E_a) over Ru/RGO and Ru/AC catalysts were investigated for better understanding the intrinsic activities of these two catalysts (Table 2, Figures S4-S7). The TOF values over Ru/RGO are 3-5 times those over Ru/AC, and E_a over Ru/RGO is lower than that over Ru/AC. This result clearly demonstrates the higher intrinsic activity of Ru/RGO. In particular, the E_a value on Ru/RGO is close to that on highly active homogeneous catalysts (61 kJ/mol)⁴⁵, indicating the unique talent of graphene as the support for enhancing the activity of Ru catalyst.

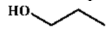
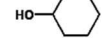
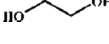
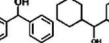
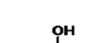
Moreover, several typical carbonyl compounds were chosen, and their hydrogenation performances on Ru/RGO catalyst were investigated (Table 3). Notably, the Ru/RGO catalyst is highly active for the hydrogenation of C=O bond in these aldehydes and ketones under mild temperatures. These

Table 2 The calculated reaction rate constants and apparent activation energies over various catalysts^a

Cat.	T/ °C	k/ h ⁻¹	TOF/ h ⁻¹	E _a (kJ/mol)
Ru/RGO	20	0.3711	2112.2 ^b	66.01
	30	0.9852	4656.3 ^c	
	40	2.0926	5520.2 ^d	
Ru/AC	20	0.0340	532.7 ^e	87.66
	30	0.1194	996.8 ^f	
	40	0.3384	1866.5 ^g	
Ru-TPPTS ^h	70	-	-	61± 2

^a: LA (2 g, 17.2 mmol), 15 g mixture of 2 wt% Ru/support catalyst and water (60 mg 2 wt% Ru/support); H₂ 4 MPa. The number of active Ru sites for TOF calculation was determined by CO pulse chemisorption. ^b: t=30 min, conversion= 40.1%; ^c: t=15 min, conversion= 44.2% ^d: t=15 min, conversion= 52.4% ^e: t=30 min, conversion= 10.9%; ^f: t=15 min, conversion= 10.2% ^g: t=15 min, conversion= 19.1% ^h: Ref. 45. The effect of H₂ on the conversion of LA was listed in Figure S3

Table 3 Hydrogenation of different carbonyl compounds over Ru/RGO catalyst ^a

Entry	reactant	product	Conv.%	Select.%	T/ °C	t/h	TOF/ h ⁻¹
1			96.6	99.9	20	4	137 ^c
2			92.8	99.8	20	4	191 ^c
3 ^b			70.1	99.8	60	3	365 ^d
4 ^b			92.3	99.9	40	1	6102 ^d
5 ^b			96.1	99.9	40	1.5	3371 ^d
6 ^b			100	96.8 ^e	40	1	2897 ^d
7 ^b			100	99.9	40	1	8296 ^d
8 ^b			100	85.6 ^f	40	1	4735 ^d

Reaction conditions: ^a: 0.2 g substrate, H₂ 0.5 MPa, 9.8 g mixture of 2 wt% Ru/RGO and water (60 mg 2 wt% Ru/RGO), ^b: 1 g substrate, 8 g ethanol; H₂ 4 MPa, 2%Ru/RGO 60 mg; ^c: t=30min ^d: 2 g substrate, 8 g ethanol; H₂ 4 MPa, 2 wt% Ru/RGO 60 mg t=20 min; ^e and ^f: the total selectivity of the two products. The carbon balance for each run exceeds 95%.

aldehydes and ketones were converted to their corresponding alcohols with high efficiency. In particular, the TOF values for the hydrogenation of furfural, acetophenone, benzophenone and acetone over Ru/RGO are much higher than those over heterogeneous catalysts reported in the literature⁴⁶⁻⁴⁹. Therefore, the Ru/RGO catalyst shows great potential as an effective and versatile catalyst for low-temperature hydrogenation of carbonyl compounds.

XRD, XPS, TEM and High-resolution TEM (HRTEM) were carried out to understand the effect of graphene support on the structure of Ru. The diffraction peak (002) of raw graphite at 26.5° disappeared after oxidation into GO (Figure S8A-b). This result indicates that the oxidation process led to the formation of few-layer graphene structure and the introduction of plenty oxygenic functional groups on the layers. These surface functional groups, as indicated by XPS results (Fig. S9a and Table S1), include C-O (hydroxyl/ epoxy), C=O (carbonyl) and O-C=O (carboxyl) (286.5, 287.4 eV and 288.5 respectively)⁵⁰⁻⁵¹. They are reported to be anchoring sites for metal complexes⁵². To verify which oxygenated functional groups are anchoring sites for Ru, Ru/RGO and RGO were analyzed by XPS (Figure S2a and Figure S9b). For RGO, the peak associated with C-C bond (centered at 284.6 eV) became predominant while the peaks of oxygenated groups (hydroxyl, epoxy, carbonyl and carboxyl) decreased tremendously compared with GO. This result suggested that most of the oxygenated groups have been removed during the reduction process (Figure S9c). For Ru/RGO, the intensities of the oxygenic functional groups were further decreased compared with RGO (Table S1). In particular, the amounts of C-O and C=O decreased obviously compared with RGO. Hence, the C-O and C=O groups are primarily the anchoring sites for Ru species. This result is in accordance with the literature⁵². These functional groups promoted the dispersion of Ru. As

indicated by XRD, the diffraction peaks of Ru nanoparticles in Ru/RGO were not detected, indicating that the particle size of Ru were below the XRD detection line (3-5 nm) (Figure S8A-d). TEM and HRTEM results imply the formation of uniformly dispersed Ru nanoparticles with an average diameter of 2.0 nm (Figure S10 a-d).

The structural evolution of graphene during the reduction was also investigated by Raman spectra. The integrated intensity ratio of D band (1350 cm⁻¹) to G band (1580 cm⁻¹) (I_D/I_G) are demonstrated to present the disorder of graphene⁵³⁻⁵⁴. After the same reduction process, the calculated I_D/I_G ratio of Ru/RGO (1.39) is larger than that of RGO (1.18) (Figure S11). This enhancement in the I_D/I_G ratio is indicative of the presence of carbon vacancies and defects that were

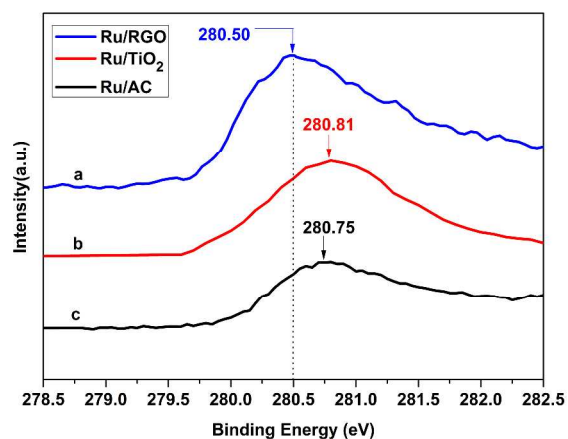


Figure 1 The XPS Ru⁰ regions of Ru supported catalyst. (a) Ru/RGO (b)Ru/TiO₂ (c) Ru/AC

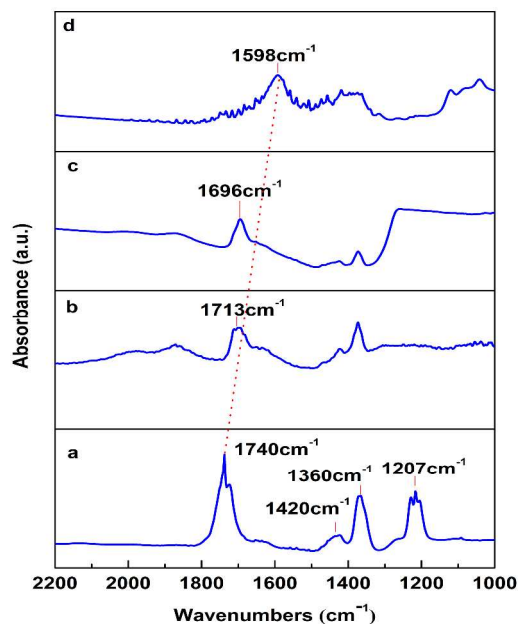


Figure 2 In situ FTIR of (a) acetone, (b) adsorbed on Ru/TiO₂, (c) adsorbed on Ru/AC, (d) adsorbed on Ru/RGO at ambient temperature.

formed during the chemical reduction of GO^{55,56}. Hence, the increased I_D/I_G ratio in Ru/RGO indicates that the reduction of GO was promoted in the presence of Ru, leading to the formation of more defects in RGO. As confirmed by HRTEM the Ru nanoparticles reduce the aggregation and restacking of graphene in the reduction process (Figure S10, a, e and f)⁵². This inhabitation effect of Ru on the aggregation of RGO was further verified by the BET results. As shown in Table S2, the S_{BET} of RGO is smaller than that of Ru/RGO.

More importantly, the XPS results of the reduced Ru catalysts provide basic clues concerning the interaction between support and Ru. Ru/RGO, Ru/AC and Ru/TiO₂ were chosen for the XPS characterization because of their obvious difference in the low-temperature activities. The overlapping of the Ru_{3d}3/2 XPS signals with the main signal of C_{1s} allows the study of metallic Ru only via the Ru_{3d}5/2 XPS signal. Dumesic et al. have reported that the temperature exceeded 140 °C is enough for reducing the supported Ru-carbon catalyst⁴¹. To clarify whether the three catalysts are fully reduced at 150 °C 4 MPa H₂, the LA hydrogenation performances and XPS spectra of the three Ru supported catalysts reduced at 150, 200 and 250 °C were investigated respectively (The reduction processes are detailed in S1.2 Method part in ESI). For each catalyst, the activities for LA hydrogenation were at the same level (Table S3), and the binding energy (BE) values of Ru⁰ nanoparticles were nearly the same at the three reduction temperatures (Figure 1, Figure S12). This result indicates that the temperature of 150 °C is sufficient for the reduction of Ru species on the three supports (RGO, AC and TiO₂). An interesting feature is the negative correlation between the BE values of Ru⁰ and low-temperature activities. As shown in Figure 1, the BE value of Ru⁰ nanoparticles on graphene is the lowest (280.50 eV), followed by those on AC (280.75 eV) and TiO₂ (280.81 eV), while Ru/RGO shows the highest low-temperature activity, followed by Ru/AC and Ru/TiO₂ (Table 1). As the BE value indicates the electron density of Ru⁰, this result suggests the electron-rich state of Ru⁰ NPs on gra-

phene. The structures of Ru nanoparticles on AC were also investigated by HRTEM and XRD (Figure S13). HRTEM and XRD results in this work and in our latest work indicate that Ru nanoparticles on AC and TiO₂ supports^{43, 44a} have similar size distribution (around 2.0 nm) and expose the same planes (002 and 100 planes) with those on graphene. It is therefore likely that the significantly higher low-temperature activity of Ru/RGO is due to the electron-rich state of Ru⁰ NPs on graphene.

To further understand the origin of the higher low-temperature activity of Ru/RGO catalyst, the activation behaviors of C=O bond on Ru/RGO, Ru/TiO₂ and Ru/AC catalyst were characterized by *in situ* Fourier-transform infrared spectroscopy (FT-IR). Acetone was chosen as the probe molecular, and the FT-IR spectra were recorded under room temperature. For acetone, the peak appearing at 1740 cm⁻¹ region is ascribed to C=O stretching vibration (Figure 2a)⁵⁷. A red shift in the wavenumber of C=O stretching vibration peak occurred in three Ru supported catalysts. Surprisingly, the red shift for Ru/RGO catalyst (142 cm⁻¹ Figure 2d) is much larger than that for Ru/TiO₂ (27 cm⁻¹ Figure 2b) and Ru/AC catalysts (44 cm⁻¹ Figure 2c). The red shift of C=O bond can be interpreted as the increase in the backbonding from Ru *d* orbital into the C=O 2π* antibonding orbital, leading to weakness in the strength of C=O bond. This result confirms apparently that the activation of C=O bonds are more effective on Ru/RGO catalyst. The highly effective activation of C=O bonds on Ru/RGO likely results from that the electron-rich state of Ru⁰ NPs on graphene promotes the electron transfer from Ru⁰ *d* orbital to C=O 2π* antibonding orbital.

The stability of the Ru/RGO catalyst was investigated by four consecutive catalytic runs at different LA conversion levels (Figure 3). GVL yield are sustained on multiple reuse. The possible Ru leaching during the reaction was also detected. As the loss of Ru is usually more severe at higher temperatures, we analyzed the amount of Ru in the solution by ICP-OES and by a reaction test at 40 °C (detailed in supporting information). No Ru was detected, reflecting that the possible leaching of Ru is below the detection limit (1 μg Ru/L solution). Furthermore, the Ru nanoparticles size of spent catalyst increased slightly from 2.0 nm to 2.5 nm (Figure S14). The above results demonstrate the excellent stability and reusability of Ru/RGO catalyst.

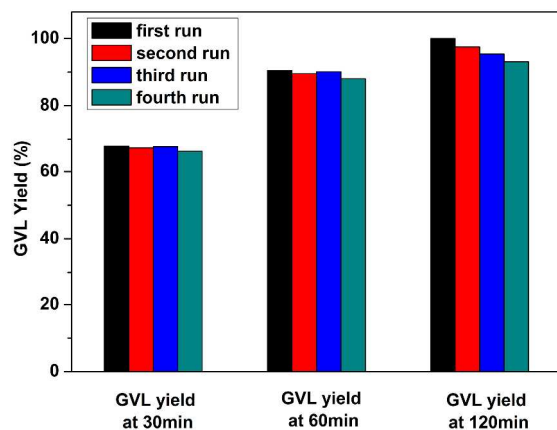


Figure 3 Stability of the Ru/RGO catalyst. Reaction conditions: LA (2 g, 17.2 mmol), 15 g mixture of 2 wt% Ru/RGO catalyst and water (60 mg 2 wt% Ru/RGO); H₂ 4 MPa.

3. Conclusion

In conclusion, the Ru/RGO catalyst exhibits remarkable efficiency for low-temperature hydrogenation of LA into GVL. GVL was obtained efficiently over the catalyst with a high yield of 99.9% and a TOF of 2112.2 h⁻¹ at room temperature (20 °C). The value of E_a for LA hydrogenation over Ru/RGO is 66.01 kJ/mol, which is equivalently to that over highly active homogeneous Ru-TPPTS catalyst (61 kJ/mol). The hydrogenation of LA can be efficiently performed at -10 °C on the catalyst. Moreover, the catalyst is also highly active towards the selective hydrogenation of C=O bonds of other carbonyl compounds into C-OH bonds. The high efficiency of the catalyst could be attributed to that the electron transferring between Ru⁰ and RGO leads to the formation of electron-rich state of Ru⁰ nanoparticles that are demonstrated to be highly active towards the activation of C=O bonds.

4. Experiment Section

4.1 Graphene oxide (GO) synthesis. GO was synthesized from graphite powder by the Hummers and Offemann's method⁵⁸. Typically, Graphite powder (4 g) and NaNO₃ (2 g) were mixed with H₂SO₄ (92 mL, 98%) under magnetic stirring at 0 °C for 1 h. KMnO₄ (12 g) was added slowly to the mixture with vigorous stirring at 10 °C. The mixture was transferred to a water bath of 35 °C for 0.5 h followed by adding a certain amount of distilled water (184 mL). The temperature of the diluted suspension was raised to 98 °C and maintained for 1 h. The suspension was further diluted to 460 mL with warm water, followed by the addition of 30% H₂O₂ aqueous solution (40 mL). Finally, the obtained solution was filtered and washed with HCl (1 mol/L) and distilled water, respectively. The resulting solid was dried and dissolved with water. The prepared suspension was ultrasonicated under 40 KHz for 60 min and centrifugated at 4000 rpm for 30 min to obtain stable collosol of GO. The collosol of GO was dried at ambient temperature to obtain power of GO.

4.2 Synthesis of Ru/RGO. Ru/RGO heterogeneous catalyst was synthesized through a hydrothermal method with hydrogen. Typically, 720 mg of as-prepared GO was dispersed into 120 mL water solution and ultrasonicated under 40 KHz for 3 h. Then 9.8 mL of as-prepared GO aqueous solution and 1.20 mL RuCl₃·3H₂O (C_{Ru3+} = 1.0 mg/ml) were added into a vessel, followed by ultrasonication for 3 h. The mixture was then stirred at room temperature overnight. Afterwards, the mixture was transferred into a Teflon-lined steel autoclave and maintained at 150 °C and 4.0 MPa H₂ for 2 h to co-reduce the GO and Ru³⁺, followed by cooling down to reaction temperature. The effect of Cl⁻ on the activity of Ru/RGO was investigated (Table S5). A certain amount of HCl (2 times the mole of Cl⁻ ions in RuCl₃·3H₂O applied for the preparation of Ru/RGO) was added into the mixture of Ru/RGO, levulinic acid and water prior to the reaction. The changes in the conversion were negligible after the addition of Cl⁻, indicating that Cl⁻ ions did not affect the activity of Ru/RGO.

4.3 Preparation of Ru/AC, Ru/TiO₂ and Ru/Graphite. The catalysts were prepared by the wet impregnation method. The support of active carbon, TiO₂ and Graphite were dried at 100 °C overnight before the wet impregnation. The dried supports were impregnated with an aqueous solution con-

taining RuCl₃·3H₂O at room temperature for 24 h, respectively, then dried at 100 °C for 20 h. Ru/TiO₂ catalyst was calcined in air at 400 °C for 4 h, while Ru/AC and Ru/Graphite were calcined in N₂ at 400 °C for 4 h. Prior to the reactions, these catalysts were moved to an autoclave and reduced at 150 °C in 4 MPa of hydrogen for 2 h in the presence of water.

4.4 Catalyst testing. All experiments were performed in a batch reactor with a magnetic stirring. Typically, LA (2 g, 17.2 mmol) was added into the Teflon-lined steel autoclave vessel with 60 mg reduced Ru catalyst and 14.94 g water. Before each run the vessel was sealed and flushed with H₂ to exclude air for five times. After reactions, the vessel was cooled down/warmed up to room temperature by water. The reaction products were centrifuged for 10 min and then filtrated to obtain clear solution. The samples were analyzed by a GC (Agilent 7890) equipped with an AB-INNOWAX capillary column (30m×0.32mm×0.5μm). Standard solutions were used to obtain the calibration curves to calculate concentrations of the compounds by the external standard method. The catalyst was recycled as described by the following procedure. At the end of the hydrogenation run, the catalyst was separated from the reaction mixture by high rate of centrifugation, thoroughly washed with water three times to remove the adsorbed species, and then reused as the catalyst for the next run under the identical conditions. The Ru content in the remained reaction solution was analyzed by ICP-OES (PerkinElmer Optima 2100 DV).

4.5 Catalyst characterizations. The catalyst characterizations are detailed in the electronic supporting information, which include (X-ray diffraction (XRD) Transmission electron microscope (TEM), high-resolution transmission electron microscope (HRTEM), X-ray photoelectron spectroscopy (XPS), BET, CO pulse chemisorption, Raman spectroscopy, and *in situ* FTIR.

ASSOCIATED CONTENT

Supporting Information. Experimental details, Table S1-S5, Figure S1 to S14 can be found in Supporting Information. This material is available free of charge via the Internet at <http://pubs.acs.org>.

AUTHOR INFORMATION

Corresponding Author

* E-mail: zhuyulei@sxicc.ac.cn (Y. Zhu). Tel.: +86 351 7117097; Fax: +86 351 7560668.

Notes

The authors declare no competing financial interest.

ACKNOWLEDGMENT

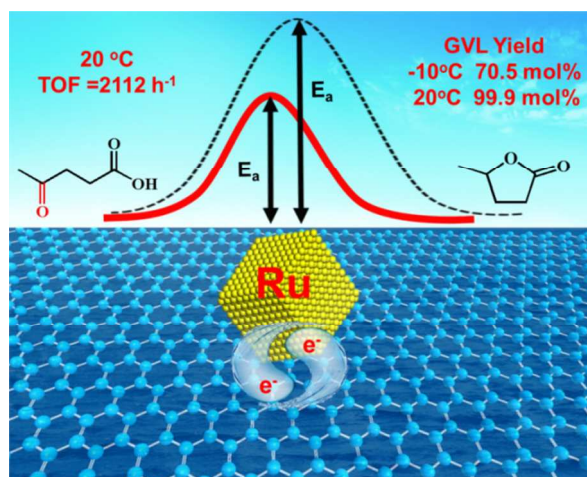
The authors gratefully acknowledge the financial support of the Major State Basic Research Development Program of China (973 Program) (no. 2012CB215305)

REFERENCES

1. Deng, J.; Li, H.; Xiao, J.; Tu, Y.; Deng, D.; Yang, H.; Tian, H.; Li, J.; Ren, P.; Bao, X. *Energy Environ. Sci.* **2015**, *8*, 1594-1601.

2. Wei, H.; Liu, X.; Wang, A.; Zhang, L.; Qiao, B.; Yang, X.; Huang, Y.; Miao, S.; Liu, J.; Zhang, T. *Nat. Chem.* **2014**, *5*, 5634-5641.
3. Shin, S. I.; Go, A.; Kim, I. Y.; Lee, J. M.; Lee, Y.; Hwang, S.-J. *Energy Environ. Sci.* **2013**, *6*, 608-617.
4. Lei, Y.; Mehmood, F.; Lee, S.; Greeley, J.; Lee, B.; Seifert, S.; Winans, R. E.; Elam, J. W.; Meyer, R. J.; Redfern, P. C.; Teschner, D.; Schlögl, R.; Pellin, M. J.; Curtiss, L. A.; Vajda, S. *Science* **2010**, *328*, 224-228.
5. Corma, A.; Serna, P.; Calvino, J. J. *J. Am. Chem. Soc.* **2008**, *130*, 8748-8753.
6. Balaraman, E.; Gunanathan, C.; Zhang, J.; Shimon, L. J. W.; Milstein, D. *Nat. Chem.* **2011**, *3*, 609-614.
7. Huff, C. A.; Sanford, M. S. *J. Am. Chem. Soc.* **2011**, *133*, 18122-18125.
8. Deng, L.; Li, J.; Lai, D.; Fu, Y.; Guo, Q. *Angew. Chem. Int. Ed.* **2009**, *48*, 6529-6532.
9. Liao, F.; Huang, Y.; Ge, J.; Zheng, W.; Tedsree, K.; Collier, P.; Hong, X.; Tsang, S. C. *Angew. Chem. Int. Ed.* **2011**, *50*, 2162-2165.
10. Vilé, G.; Colussi, S.; Krumeich, F.; Trovarelli, A.; Pérez-Ramírez, J. *Angew. Chem. Int. Ed.* **2014**, *53*, 12069-12072.
11. Xie, X.; Li, Y.; Liu, Z.; Haruta, M.; Shen, W. *Nature* **2009**, *458*, 746-749.
12. Li, Y.; Shen, W. *Chem. Soc. Rev.* **2014**, *43*, 1543-1574.
13. Qiao, B.; Wang, A.; Yang, X.; Allard, L. F.; Jiang, Z.; Cui, Y.; Liu, J.; Li, J.; Zhang, T. *Nat. Chem.* **2011**, *3*, 634-641.
14. Vayssilov, G. N.; Lykhach, Y.; Migani, A.; Staudt, T.; Petrova, G. P.; Tsud, N.; Skála, T.; Bruix, A.; Illas, F.; Prince, K. C.; Matolín, V.; Neyman, K. M.; Libuda, J. *Nat. Mater.* **2011**, *10*, 310-315.
15. Anderson, P. E.; Rodríguez, N. M. *Chem. Mater.* **2000**, *12*, 823-830.
16. Liu, X.; Wang, A.; Zhang, T.; Mou, C. *Nano Today* **2013**, *8*, 403-416.
17. Campbell, C. T. *Nat. Chem.* **2012**, *4*, 597-598.
18. Wang, L.; Meric, I.; Huang, P.; Gao, Q.; Gao, Y.; Tran, H.; Taniguchi, T.; Watanabe, K.; Campos, L. M.; Müller, D. A.; Guo, J.; Kim, P.; Hone, J.; Shepard, K. L.; Dean, C. R. *Science* **2013**, *342*, 614-617.
19. Gao, L.; Ren, W.; Xu, H.; Jin, L.; Wang, Z.; Ma, T.; Ma, L.; Zhang, Z.; Fu, Q.; Peng, L.; Bao, X.; Cheng, H. *Nat. Commun.* **2012**, *3*, 699-705.
20. Novoselov, K. S.; Fal'ko, V. I.; Colombo, L.; Gellert, P. R.; Schwab, M. G.; Kim, K. *Nature* **2012**, *490*, 192-200.
21. Balandin, A. A. *Nat. Mater.* **2011**, *10*, 569-581.
22. Huang, C.; Li, C.; Shi, G. *Energy Environ. Sci.* **2012**, *5*, 8848-8868.
23. Chang, H.; Wu, H. *Energy Environ. Sci.* **2013**, *6*, 3483-3507.
24. Stoller, M. D.; Park, S.; Zhu, Y.; An, J.; Ruoff, R. S. *Nano Lett.* **2008**, *8*, 3498-3502.
25. Dean, C. R.; Young, A. F.; Cadden-Zimansky, P.; Wang, L.; Ren, H.; Watanabe, K.; Taniguchi, T.; Kim, P.; Hone, J.; Shepard, K. L. *Nat. Phys.* **2011**, *7*, 693-696.
26. Rao, C. N. R.; Sood, A. K.; Subrahmanyam, K. S.; Govindaraj, A. *Angew. Chem. Int. Ed.*, **2009**, *48*, 7752-7777.
27. Novoselov, K. S. *Science* **2007**, *315*, 1379.
28. Liu, X.; Yao, K.; Meng, C.; Han, Y. *Dalton Trans.* **2012**, *41*, 1289-1296.
29. Gong, C.; Lee, G.; Shan, B.; Vogel, E. M.; Wallace, R. M.; Cho, K. *J. Appl. Phys.* **2010**, *108*, 123711-123718.
30. Wang, B.; Günther, S.; Wintterlin, J.; Bocquet, M. L. *New J. Phys.* **2010**, *12*, 043041-043055.
31. Khomyakov, P. A.; Giovannetti, G.; Rusu, P. C.; Brocks, G.; van den Brink, J.; Kelly, P. J. *Phys. Rev. B.* **2009**, *79*, 195425-195436.
32. Yang, J.; Sun, G.; Gao, Y.; Zhao, H.; Tang, P.; Tan, J.; Lu, A.; Ma, D. *Energy Environ. Sci.* **2013**, *6*, 793-798.
33. Corma, A.; Iborra, S.; Velty, A. *Chem. Rev.* **2007**, *107*, 2411-2502.
34. Wettstein, S. G.; Alonso, D. M.; Chong, Y.; Dumesic, J. A. *Energy Environ. Sci.* **2012**, *5*, 8199-8203.
35. Weingarten, R.; Conner, W. C.; Huber, G. W. *Energy Environ. Sci.* **2012**, *5*, 7559-7574.
36. a) Tang, X.; Zeng, X.; Li, Z.; Hu, L.; Sun, Y.; Liu, S.; Lei, T.; Lin, L. *Renew. Sust. Energ. Rev.* **2014**, *40*, 608-620; b) Wright, W. R. H.; Palkovits, R. *ChemSusChem* **2012**, *5*, 1657-1667.
37. a) Yuan, J.; Li, S.; Yu, L.; Liu, Y. M.; Cao, Y.; He, H.; Fan, K. *Energy Environ. Sci.* **2013**, *6*, 3308-3313; b) Shimizu, K. I.; Kanno, S.; Kona, K. *Green Chem.* **2014**, *16*, 3899-3903; c) Zhou, H.; Song, J.; Fan, H.; Zhang, B.; Yang, Y.; Hu, J.; Zhu, Q.; Han, B. *Green Chem.* **2014**, *16*, 3870-3875.
38. a) Sudhakar, M.; Vijay Kumar, V.; Naresh, G.; Lakshmi Kantam, M.; Bhargava, S.K.; Venugopal, A. *Appl. Catal. B: Environ.* **2016**, *180*, 113-120; b) Abdelrahman, O. A.; Heyden, A.; Bond, J. Q. *ACS Catal.* **2014**, *4*, 1171-1181; c) Yang, Y.; Gao, G.; Zhang, X.; Li, F. *ACS Catal.* **2014**, *4*, 1419-1425; d) Al-Shaal, M. G.; Wright, W. R. H.; Palkovits, R. *Green Chem.* **2012**, *14*, 1260-1263.
39. a) Mehdi, H.; Fábos, V.; Tuba, R.; Bodor, A.; Mika, L. T.; Horváth, I. T. *Top. Catal.* **2008**, *48*, 49-54; b) Fábos, V.; Mika, L. T.; Horváth, I. T. *Organometallics* **2014**, *33*, 181-187; c) Tukacs, J. M.; Király, D.; Strádi, A.; Novodarszki, G.; Eke, Z.; Dibó, G.; Kégl, T.; Mika, L. T. *Green Chem.* **2012**, *14*, 2057-2065.

- 1 40. a) Ortiz-Cervantes, C.; Flores-Alamo, M.; GarcíaUpare, J. J.
2 *ACS Catal.* **2015**, *5*, 1424-1431; b) Liguori, F.; Moreno-Marrodan,
3 C.; Barbaro, P. *ACS Catal.* **2015**, *5*, 1882-1894; c) Tukacs, J. M.;
4 Novák, M.; Dibób, G.; Mika, L. T. *Catal. Sci. Technol.* **2014**, *4*,
5 2908-2912; d) Qi, L., Horváth, I. T. *ACS Catal.* **2012**, *2*, 2247-
6 2249
- 7 41. Braden, D. J.; Henao, C. A.; Heltzel, J.; Maravelias, C. C.;
8 Dumesic, J. A. *Green Chem.* **2011**, *13*, 1755-1765.
- 9 42. Luo, W.; Sankar, M.; Beale, A. M.; He, Q.; Kiely, C. J.;
10 Bruijninx, P. C. A.; Weckhuysen, B. M. *Nat. Commun.* **2015**, *6*,
11 6540-6549.
- 12 43. Cui, J.; Tan, J.; Deng, T.; Cui, X.; Zheng, H.; Zhu, Y.; Li, Y.
13 *Green Chem.* **2015**, *17*, 3084-3089.
- 14 44. a) Tan, J.; Cui, J.; Deng, T.; Cui, X.; Ding, G.; Zhu Y.; Li, Y.
15 *ChemCatChem* **2015**, *7*, 508-512; b) Tan, J.; Cui, J.; Ding, G.;
16 Deng, T.; Zhu Y.; Li, Y. *Catal. Sci. Technol.* **2015**, DOI:
17 10.1039/C5CY01374G.
- 18 45. Chalid, M.; Broekhuis, A. A.; Heeres, H. J. *J. Mol. Catal. A:*
19 *Chem.* **2011**, *341*, 14-21.
- 20 46. Yuan, Q.; Zhang, D.; Haandel, L.; Ye, F.; Xue, T.; Hensen, E.
21 J. M.; Guan, Y. *J. Mol. Catal. A: Chem.* **2015**, *406*, 58-64.
- 22 47. Yoshida, H.; Onodera, Y.; Fujita, S. I.; Kawamori, H.; Arai,
23 M. *Green Chem.* **2015**, *17*, 1877-1883.
- 24 48. Albrecht, M.; Crabtree, R. H.; Mata, J.; Peris, E. *Chem. Com-*
25 *mun.* **2002**, 32-33.
- 26 49. Van Druten, G. M. R.; Ponec, V. *Appl. Catal. A: Gen.*
27 **2000**, *191*, 153-162.
- 28 50. Park, S.; An, J.; Potts, J. R.; Velamakanni, A.; Murali, S.;
29 Ruoff, R. S. *Carbon* **2011**, *49*, 3019-3023.
- 30 51. Park, S.; Lee, K.-S.; Bozoklu, G.; Cai, W.; Nguyen, S. T.;
31 Ruoff, R. S. *ACS nano.* **2008**, *3*, 572-578.
- 32 52. Li, Y.; Gao, W.; Ci, L.; Wang, C.; Ajayan, P. M. *Carbon*
33 **2010**, *48*, 1124-1130.
- 34 53. Ferrari, A. C.; Basko, D. M. *Nat. Nano.* **2013**, *8*, 235-246.
- 35 54. Eckmann, A.; Felten, A.; Mishchenko, A.; Britnell, L.;
36 Krupke, R.; Novoselov, K. S.; Casiraghi, C. *Nano Lett.* **2012**, *12*,
37 3925-3930.
- 38 55. a) Kundu, P.; Nethravathi, C.; Deshpande, P. A.; Rajamathi,
39 M.; Madras, G.; Ravishankar, N. *Chem. Mater.* **2011**, *23*, 2772-
40 2780; b) Shi, J.; Nie, R.; Chen, P.; Hou, Z. *Catal. Commun.* **2013**,
41 *41*, 101-105;
- 42 56. Bagri, A.; Mattevi, C.; Acik, M.; Chabal, Y. J.; Chhowalla, M.;
43 Shenoy, V. B. *Nat. Chem.* **2010**, *2*, 581-587.
- 44 57. Centeno, M. A.; Montes, M.; Fernandez Sanz, J.; Odriozola, J.
45 A. *Mater. Sci. Forum* **2002**, *383*, 105-110.
- 46 58. Hummers, W. S.; Offeman, R. E. *J. Am. Chem. Soc.* **1958**, *80*,
47 1339-1339.
- 48
49
50
51
52
53
54
55
56
57
58
59
60



The high efficiency of graphene-modified Ru nanocatalyst for low-temperature hydrogenation of C=O bonds originates from the electron transfer between Ru⁰ and graphene.